Bioactive Materials 5 (2020) 636–643

Contents lists available at ScienceDirect

Bioactive Materials

journal homepage: http://www.keaipublishing.com/biomat

3D printing of multilayered scaffolds for rotator cuff tendon regeneration

Xiping Jiang[a,b], Shaohua Wu[a,c], Mitchell Kuss[a], Yunfan Kong[a], Wen Shi[a], Philipp N. Streubel[d], Tieshi Li[e], Bin Duan[a,f,g,*]

[a] Mary & Dick Holland Regenerative Medicine Program, Division of Cardiology, Department of Internal Medicine, University of Nebraska Medical Center, Omaha, NE, 68198, USA
[b] Molecular Genetics and Cell Biology Program, Department of Genetics, Cell Biology and Anatomy, University of Nebraska Medical Center, Omaha, NE, 68198, USA
[c] College of Textiles & Clothing, Collaborative Innovation Center of Marine Biomass Fibers, Qingdao University, Qingdao, 266071, China
[d] Department of Orthopedic Surgery and Rehabilitation, University of Nebraska Medical Center, Omaha, NE, 68198, USA
[e] Department of Pediatrics, University of Nebraska Medical Center, Omaha, NE, 68198, USA
[f] Department of Surgery, College of Medicine, University of Nebraska Medical Center, Omaha, NE, 68198, USA
[g] Department of Mechanical and Materials Engineering, University of Nebraska-Lincoln, Lincoln, NE, 68516, USA

ARTICLE INFO

Keywords:
Collagen-fibrin hydrogel
Tenogenic differentiation
Tendon repair
Tissue engineering

ABSTRACT

Repairing massive rotator cuff tendon defects remains a challenge due to the high retear rate after surgical intervention. 3D printing has emerged as a promising technique that enables the fabrication of engineered tissues with heterogeneous structures and mechanical properties, as well as controllable microenvironments for tendon regeneration. In this study, we developed a new strategy for rotator cuff tendon repair by combining a 3D printed scaffold of polylactic-*co*-glycolic acid (PLGA) with cell-laden collagen-fibrin hydrogels. We designed and fabricated two types of scaffolds: one featuring a separate layer-by-layer structure and another with a tri-layered structure as a whole. Uniaxial tensile tests showed that both types of scaffolds had improved mechanical properties compared to single-layered PLGA scaffolds. The printed scaffold with collagen-fibrin hydrogels effectively supported the growth, proliferation, and tenogenic differentiation of human adipose-derived mesenchymal stem cells. Subcutaneous implantation of the multilayered scaffolds demonstrated their excellent *in vivo* biocompatibility. This study demonstrates the feasibility of 3D printing multilayered scaffolds for application in rotator cuff tendon regeneration.

1. Introduction

The prevalence of rotator cuff tendon tears among all age groups is around 34%, with a likelihood of 50% for people after the age of sixty years old [1,2]. Rotator cuff tendon injuries are associated with more than 4.5 million physician visits and 40,000 surgical treatments annually in the United States [3,4]. Aging, tear size, and fat infiltration are three main risk factors for the progression of rotator cuff tendon tears [5]. In most cases, the initial region of rotator cuff tears starts near the insertion of supraspinatus and infraspinatus tendons [6]. Depending on the tear size, rotator cuff tendon tears can be classified into four types: small < 1 cm, medium 1–3 cm, large 3–5 cm, and massive > 5 cm [7,8]. Approximately 30% of rotator cuff injuries are considered irreparable due to large and massive tears [9]. Despite surgical intervention, the rate of retear is ~7% for all age groups, and the rate for people aged > 70 years old is as high as 25% [10,11]. Due to the high failure rate, massive rotator cuff tendon tear repairs remain a challenge.

Multiple strategies have been studied to reconstruct the torn rotator cuff tendon, like autografts, allografts, xenografts, and synthetic materials [12]. However, there are still many potential problems when using these grafts. For example, autografts, like latissimus dorsi transfer and pectoralis major transfer, have a relatively high failure rate due to mismatched mechanical properties and possible morbidity and anatomical damage at the donor site [13,14]. For allografts, the remaining donor DNA could cause inflammation and an immune response, accelerating the rate of graft degeneration and inducing edema at the surgical site [15,16]. Xenografts, like porcine dermal collagen implants and small intestine submucosa, have not been thoroughly studied, and some resulted in unfavorable outcomes [17,18]. In comparison, biomaterials-based strategies for rotator cuff repair can strengthen the

Peer review under responsibility of KeAi Communications Co., Ltd.
* Corresponding author. Mary & Dick Holland Regenerative Medicine Program; Division of Cardiology, Department of Internal Medicine, University of Nebraska Medical Center, Omaha, NE, 68198, USA.
E-mail address: bin.duan@unmc.edu (B. Duan).

https://doi.org/10.1016/j.bioactmat.2020.04.017
Received 27 March 2020; Received in revised form 23 April 2020; Accepted 23 April 2020

mechanical elasticity and stability of the rotator cuff tendon without a severe immune response [19–21]. Currently, there are three types of commonly-used polymers for rotator cuff tendon repair: natural biomaterials (e.g. chitosan [22], collagen [23], fibrin [24], and silk fibroin [25]), synthetic degradable polymers (e.g. poly-lactic acid (PLA) [26], polylactic-*co*-glycolic acid (PLGA) [27,28]), and non-degradable polymers (e.g. polyurethane [29]).

3D printing has emerged as a promising technique to fabricate highly ordered scaffolds with complex shapes [30]. Compared with traditional techniques, like conventional textiles and electrospinning, 3D printing can fabricate scaffolds with more precise pore size and geometry, better imitate the 3D structure of the extracellular matrix, and enable high mechanical properties [31]. Importantly, many 3D printers now support the implementation of multiple biomaterials to 3D print/bioprint constructs with heterogeneous structures or interfaces [32,33]. However, scaffolds 3D printed by biologically inactive synthetic materials alone cannot provide sufficient support for functional regeneration. Many biological factors, like growth factors and living cells, have been incorporated to further improve the scaffold functions [34]. Mesenchymal stem cells (MSCs) have been reported to improve the tendon healing process through accelerating the matrix synthesis, re-colonizing injured tissues, and modulating the immune response [35]. Studies have also shown that surgical augmentation with the incorporation of MSCs contributed to reduced retear rate [36,37]. Collagen and fibrin have been used individually or together as biomaterials with MSCs because of their effective interaction with embedded cells [38]. Collagen-fibrin hydrogels can further improve stem cell function and tissue remodeling via facilitating cell spreading and proliferation [39].

In this study, we aimed to develop multilayered scaffolds that can incorporate MSCs and simultaneously meet the requirements of biomechanical strength and biological function. We used two strategies, i.e., one featuring a separate layer-by-layer structure and the other with a tri-layered structure as a whole, to generate 3D-printed multilayered PLGA scaffolds combined with human adipose derived MSCs (hADMSCs) embedded in a collagen-fibrin hydrogel for tendon regeneration. We characterized the mechanical properties of these two scaffold models and investigated their biological effects on cell growth, proliferation, tenogenic differentiation, and tissue compatibility.

2. Materials and methods

2.1. Fabrication of two PLGA scaffold models by 3D printing

Two scaffold models were established by using our extrusion-based 3D bioprinter (3D-Bioplotter® Manufacturer Series, EnvisionTEC), i.e., one featuring a separate layer-by-layer structure and the other with a tri-layered structure. In the first model, PLGA (PURASORB® PDLG 5010, LA/GA = 50/50, Corbion, Netherlands) was used as the ink to 3D print a thin layer with a designed porous structure (Fig. 1A). A collagen-fibrin hydrogel was injected by pipette on the top of the printed one-layer scaffold. The second layer of PLGA scaffold was placed on the hydrogel, followed by injecting another layer of collagen-fibrin hydrogel. The third layer of PLGA scaffold was put on the top. Therefore, the scaffolds were fabricated by stacking three layers of 3D printed PLGA scaffolds with a layer of hydrogel in between each of the PLGA layers (Fig. 1B). In the second model, tri-layered scaffolds were 3D printed by using PLGA and Pluronic F127. Both inks were printed in a parallel and cross-sectionally interlaced manner in three layers as the whole structure (Fig. 1C). Collagen-fibrin hydrogels were injected by pipette onto the printed tri-layer scaffolds (Fig. 1D). Sections 2.4 and 2.5 provide more detailed descriptions about the collagen-fibrin hydrogel preparation and injection processes with the incorporation of hADMSCs. For the ink preparation and 3D printing process, PLGA was dissolved in formic acid (Sigma, USA) at 60% (w/v), and 40% Pluronic F127 (Sigma, w/v) was dissolved in water at 4 °C. Pluronic F127 served as a sacrificial material and was dissolved in cold water after printing. For the separate layer-by-layer structure, the PLGA ink was extruded through a 25-gauge needle (0.260 mm inner diameter) using a pressure of 1.5–2.0 bar and a print head movement speed of 8 mm/s. The dimensions of the one-layer scaffold was 20 mm × 15 mm (Fig. 1A). A 0.5 mm distance printing pattern was used to create the two solid ends. Each end was printed as a 2.5 mm × 15 mm rectangle. The gaps in the middle frame were designed to be 2.2 mm. For the tri-layered structure, Pluronic F127 was extruded through another 25-gauge needle using a pressure of 1.5–2.0 bar and a print head movement speed of 11 mm/s. The two solid ends in each layer were printed in the same way and with the same size as mentioned previously for the single layer printing. PLGA and Pluronic F127 were extruded in turn to generate the middle part. The printing pattern was a 2.0 mm distance interlaced for both PLGA and Pluronic F127. The scaffold was printed with a rectangular size of 20 mm × 15 mm and a 3-layer thickness (~1.15 mm) (Fig. 1C).

2.2. Morphological and mechanical characterization of scaffolds

The morphology of a one-layer PLGA scaffold was examined by a scanning electron microscope (SEM, FEI Quanta 200, Japan) after a coating of a thin layer of gold. The mechanical properties of one-layer, separate layer-by-layer structure, and tri-layered structure scaffolds were examined by a tensile strength tester (CellScale, Canada) with a gauge length of 20 mm and a constant movement rate of 0.15 mm/s until failure occurred. We calculated the elastic stiffness of the scaffolds from the initial 5–10% strain region of the force − stain curves. The ultimate forces were also determined.

2.3. Cell culture

Primary hADMSCs (Lonza, USA) were cultured in 5% CO_2 at 37 °C in growth medium (GM) containing Dulbecco's modified Eagle's medium/F12 (DMEM/F12, Invitrogen, USA) medium, 10% fetal bovine serum (FBS, Gibco, USA), and 1% penicillin/streptomycin (P/S, Invitrogen, USA) [40].

2.4. Preparation of collagen-fibrin hydrogels with hADMSCs

All of the preparation of the collagen hydrogel was performed in an icebox. We first mixed 50 μL 10 × phosphate buffered saline solution (PBS) with 450 μL 3 mg/mL type I human collagen solution (VitroCol®, Advanced BioMatrix, USA), and then we adjusted the pH to 7.0 with 5 μL 1 mol/L NaOH solution. Human fibrinogen (EMD Millipore Corporation, USA) was dissolved in PBS at a concentration of 6 mg/mL at 37 °C. Thrombin (100 units/mL, Thermo Fisher Scientific) was diluted to 1 unit/mL in the medium with suspended hADMSCs (2×10^6/mL). For hydrogel formation, 100 μL of human collagen, 100 μL of human fibrinogen, and 100 μL of hADMSCs suspension with 1 unit/mL thrombin were mixed. The final concentrations of human collagen and fibrin were 0.9 mg/mL and 2 mg/mL, respectively.

2.5. Combination of PLGA scaffolds, collagen-fibrin hydrogels, and hADMSCs

PLGA scaffolds were cut in half equally and sterilized with UV light for 2 h, submerged in 70% (v/v) ethanol overnight, washed three times in PBS, and then immersed in GM overnight. For the separate layer-by-layer structure, 100 μL of the collagen-fibrin hydrogel and hADMSCs mixture was quickly injected by pipette onto a one-layer PLGA scaffold. Another scaffold was placed on the hydrogel, followed by injecting 100 μL of the hydrogel and cell mixture. The third layer was placed on the top. For the tri-layered structure model, 200 μL of the collagen-fibrin hydrogel and hADMSCs mixture were injected by pipette onto the whole structure. All of the scaffolds with hydrogel and hADMSCs were incubated at 37 °C for approximately 3 h to obtain polymerized

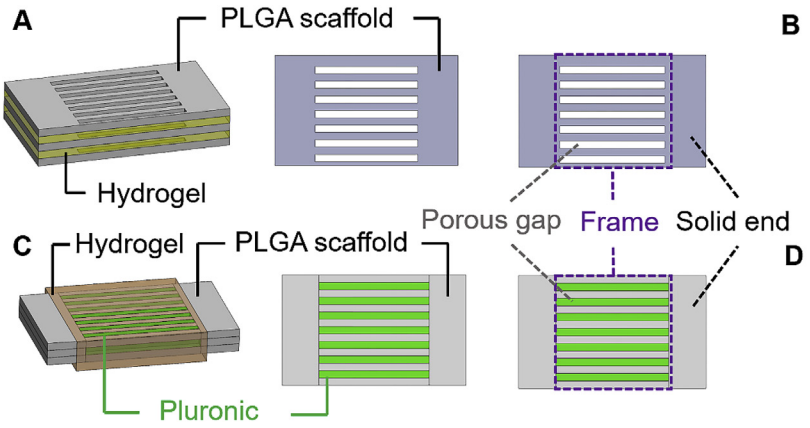

Fig. 1. Schematics of two PLGA scaffold models with collagen-fibrin hydrogels. (A) Schematic illustration of the separate layer-by-layer structure. Three layers of PLGA scaffolds sandwiched with two layers of collagen-fibrin hydrogels in between injected by pipette. (B) Final separate layer-by-layer structure of PLGA scaffolds with collagen-fibrin hydrogels. The PLGA scaffolds were cut in half equally before the collagen-fibrin hydrogels were injected. (C) Schematic illustration of the tri-layered structure. Three layers of PLGA and Pluronic F127 were printed as a whole structure. Pluronic F127 was washed out in cold water after printing. Collagen-fibrin hydrogels were injected by pipette and wrapped around the three-layer PLGA scaffolds. (D) Final tri-layered structure of PLGA scaffolds with collagen-fibrin hydrogels. The Pluronic F127 was washed out. The PLGA scaffolds were cut in half equally before the collagen-fibrin hydrogels were injected.

Table 1
Primer sequences for qPCR.

Gene symbol	Genbank ID	Primer sequences (5′→3′)	Product size (bp)
18S	NR_003286	F: GAGAAACGGCTACCACATCC R: CACCAGACTTGCCCTCCA	170
TNMD	NM_022144.2	F: AATGAACAGTGGGTGGTCCC R: TTGCCTCGACGGCAGTAAAT	164
TNC	NM_002160.3	F: AAAGCGGGGAATGTTGGGAT R: CCTGTAAGCTTTTCCCAAGTG	139
SCX	NM_001080514.2	F: AGCGATTCGCAGTTAGGAGG R: GTCTGTACGTCCGTCTGTCC	185
COL1	NM_000088.3	F: CTACGATGGCTGCACGAGTC R: GACAGGGCCAATGTCGATGC	151
COL3	NM_000090.3	F: CGCCCTCCTAATGGTCAAGG R: TTCTGAGGACCAGTAGGGCA	161

hydrogels.

2.6. Cell viability, morphology, and proliferation within hydrogel and scaffold

One-layer PLGA scaffolds with 100 μL of the collagen-fibrin hydrogel and hADMSCs were cultured together in GM and used to analyze the cell viability, morphology, and proliferation. The viability and morphology of hADMSCs were examined via a Live/Dead assay (Invitrogen, USA) after culturing in GM for 7 days, as previously described [41]. A confocal laser scanning microscope (CLSM, LSM 710, Carl Zeiss, Germany) was utilized to image the fluorescence of living and dead cells. The proliferation of hADMSCs was evaluated by an MTT assay after culturing for 3 days and 7 days, as previously described [42].

2.7. Tenogenic differentiation and immunofluorescent staining

PLGA scaffolds with the collagen-fibrin hydrogel and hADMSCs were cultured and induced in tenogenic differentiation medium (TDM). TDM consisted of DMEM/F12 medium, 2% FBS, and 20 ng/mL transforming growth factor-beta (TGFβ)3 (PeproTech, USA) [43]. The one-layer PLGA scaffolds with hydrogel and hADMSCs were cultured in TDM for 14 days, and immunofluorescent staining was conducted as previously described [44]. Briefly, the scaffold with hydrogel and hADMSCs was fixed in 4% paraformaldehyde, permeabilized in 0.2% Triton X-100, and then blocked with 1% bovine serum albumin (BSA) overnight at 4 °C. The whole system was then incubated with primary antibodies to tenomodulin (TNMD, 1:50, Abcam, USA) overnight at 4 °C, followed by secondary fluorescent antibodies for 2 h. Nuclear counterstaining (Draq 5, 1:1000, Thermo Scientific, USA) was performed at room temperature for 30 min. A Zeiss 710 CLSM was used to image the samples.

2.8. RNA isolation and qPCR

PLGA scaffolds with collagen-fibrin hydrogel and hADMSCs were cultured with and without tenogenic differentiation for qPCR testing. Total RNA was extracted from the hADMSCs embedded in the hydrogel and scaffold at day 14 for both groups via QIA-Shredder and RNeasy mini-kits (QIAgen, USA). Total RNA was reverse transcribed into first-strand cDNA using an iScript cDNA synthesis kit (BioRad Laboratories, USA). A quantitative real-time polymerase chain reaction (qPCR) was conducted in a StepOnePlus™ Real-Time PCR System (Thermo Scientific, USA) via SsoAdvanced SYBR Green Supermix (Bio-Rad, USA). The level of expression of each target gene was normalized to 18s rRNA using the comparative Ct ($2^{-\Delta\Delta Ct}$) method. All primers used were shown in Table 1.

2.9. Animals and subcutaneous implant

All animal procedures were approved by the Institutional Animal Care and Use Committee (IACUC) at the University of Nebraska Medical Center (UNMC). Two types of PLGA scaffold models with the collagen-fibrin hydrogel without hADMSCs were freeze-dried and sterilized with UV light before implantation. Three scaffolds of either model were prepared to subcutaneously implant into three BALB/cJ mice (12 weeks old). Mice were maintained under general anesthesia with oxygen and isoflurane (1–5% inhalation to effect). Carprofen was administrated before surgery. Anesthetic status was monitored by toe pinch and respiratory observation. The surgical area was shaved, sterilized with povidone-iodine and ethanol and draped in a sterile surgical manner. An incision was made on the back of the mice to detach the skin from the underlying fascia. Skin pockets on each side of the mice were enlarged using tweezers. For each mouse, one scaffold of the separate layer-by-layer structure and one scaffold of the tri-layered structure were implanted into skin pockets. The skin was closed with wound clips. Mice were euthanized by CO_2 and cervical dislocation at 14 days after surgery. The implanted scaffolds were harvested.

2.10. Histology

Harvested scaffolds were fixed in buffered formalin for 48 h at 4 °C, followed by routine dehydration and paraffin embedding. Sections with 5 μm thickness were obtained and stained with hematoxylin and eosin (H&E).

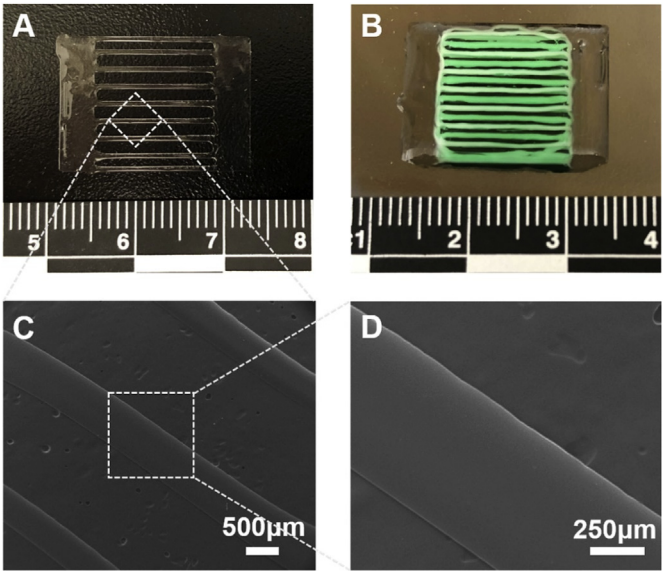

Fig. 2. Two types of 3D printed scaffolds. (A) 3D-printed one-layer PLGA scaffold for the separate layer-by-layer model. (B) 3D-printed tri-layered scaffold model using PLGA and Pluronic F127. Pluronic F127 was dyed with green food color. (C, D) SEM images of one-layer PLGA scaffold.

2.11. Statistical analysis

All quantitative data were expressed as mean ± standard deviation (SD). The MTT assay and PCR gene expression were analyzed by unpaired two sample *t*-test. Elastic stiffness and ultimate force were calculated by one-way ANOVA. Pairwise comparisons between groups were conducted using ANOVA with Tukey post hoc tests in statistical analysis. A value of $p < 0.05$ was considered statistically significant.

3. Results and discussion

3.1. Multilayered scaffold fabrication

Two types of scaffolds were designed and fabricated. Fig. 1A and B demonstrate the separate layer-by-layer model. The PLGA scaffold was printed first in a single-layer pattern (Fig. 2A). Then, three single-layered PLGA scaffolds were piled up with a collagen-fibrin hydrogel and hADMSCs in between each layer. Fig. 1C and D illustrate the tri-layered model. PLGA and Pluronic F127 were printed for three layers in a parallelly and cross-sectionally interlaced manner as a whole structure (Fig. 2B). Pluronic F127 served as a sacrificial material, which was washed out in cold water after printing. The collagen-fibrin hydrogels with hADMSCs were then wrapped around the tri-layered structure. For both models, the two solid ends were designed to be sutured to the two ends of a rotator cuff tendon defect in a future *in vivo* implantation. This design will make suturing and handling easier. The parallel frame structure in the middle part is designed to mimic the tendon structure and will be able to guide the alignment of tendon tissue. The porous gap between the frame will facilitate cell and tissue infiltration within the scaffolds. The three-layer structure reinforces the mechanical strength of the scaffolds. The separate layer-by-layer structure is printing-friendly, since it can be printed in high resolution and quality, maintaining an excellent three-layer morphology. It also enables additional modification of hydrogels between layers after the scaffolds are printed. Each layer can be further customized with composites to mimic tendon and bone tissue and further enhance the mechanical properties by combining them with other materials, like fibrous meshes. For the tri-layered structure, this design precludes potential layer delamination or structural alteration between each layer and facilitates hydrogel penetration in the parallel frame. It is also featured as being suture-friendly since the two solid ends provide a uniform structure that can prevent the layers from moving.

3.2. Surface morphology of 3D printed PLGA scaffold

The morphology of the one-layer PLGA scaffold was shown in Fig. 2C and D. The surface of the 3D-printed scaffold was very smooth. As many previous studies reported, rough or patterned surfaces may more effectively support cell adhesion than smooth surfaces of the same material [45,46]. Sadeghi et al. demonstrated that collagen modified PLGA scaffolds promoted cell adhesion and proliferation [47]. Similarly, Wang et al. showed that fibrin gel facilitated the incorporation of MSCs within a PLGA sponge for full-thickness cartilage regeneration [48]. In our current study, we used a collagen-fibrin hydrogel to promote the spreading, proliferation, and tenogenic differentiation of hADMSCs. The application of composite matrices is better than harnessing pure collagen or fibrin, since it can utilize both the mechanical and biochemical properties of these materials [49]. Christopher et al. showed that the combination of collagen and fibrin increased the gel compaction, which supported higher cell and matrix concentrations and resulted in enhanced mechanical properties [50]. The 3D printed PLGA scaffolds in this study provide the mechanical support for hydrogels and encapsulated cells.

3.3. Mechanical properties of the two types of PLGA scaffolds

The mechanical properties of the two types of 3D printed scaffolds, as well as one-layer PLGA scaffolds, were tested. The typical force−-strain curve was shown in Fig. 3A. Since it was hard to determine the cross-sectional area, we used force instead of stress and calculated the elastic stiffness rather than the Young's modulus. The elastic stiffness was calculated by the altered force divided by corresponding altered length from the initial 5–10% strain region in the force−stain curves. The elastic stiffness of the tri-layered scaffolds was higher than the separate layer-by-layer scaffolds (Fig. 3B). The ultimate force for both types of the full scaffolds were comparable, which were significantly higher than that of the one-layer PLGA scaffold (Fig. 3C). Both types of scaffolds with multiple layers displayed favorable mechanical properties. However, compared with the commercial patches and strategies currently used in the clinic, the mechanical strength of our scaffold models still needs to be improved [51,52].

3.4. PLGA scaffold with collagen-fibrin hydrogel supported hADMSCs proliferation

A PLGA scaffold with collagen-fibrin hydrogel and encapsulated hADMSCs was implemented to evaluate the cell viability and proliferation. The Live/Dead assay showed that the scaffold with hydrogel maintained the cell viability after culturing in GM for 7 days (Fig. 4A). The MTT assay demonstrated that the cell proliferation rate in the scaffold with the hydrogel system was significantly higher at day 7 than that at day 3 (Fig. 4B), indicating that the scaffold with hydrogel supported hADMSCs proliferation.

3.5. PLGA scaffold with collagen-fibrin hydrogel supported hADMSCs tenogenic differentiation

We further induced the tenogenic differentiation of hADMSCs within the collagen-fibrin hydrogel-laden PLGA scaffold. The scaffolds with hydrogel and hADMSCs were cultured in GM and TDM for 14 days. The immunofluorescent staining showed the expression of tenomodulin (TNMD, a late marker for tendon development and tenogenic differentiation) of hADMSCs after 14-day differentiation (Fig. 5A). We also evaluated the tenogenic differentiation-related gene expressions, scleraxis (SCX, a transcription factor that regulates the early tenogenic differentiation and tendon development [53]), tenascin-C (TNC, an

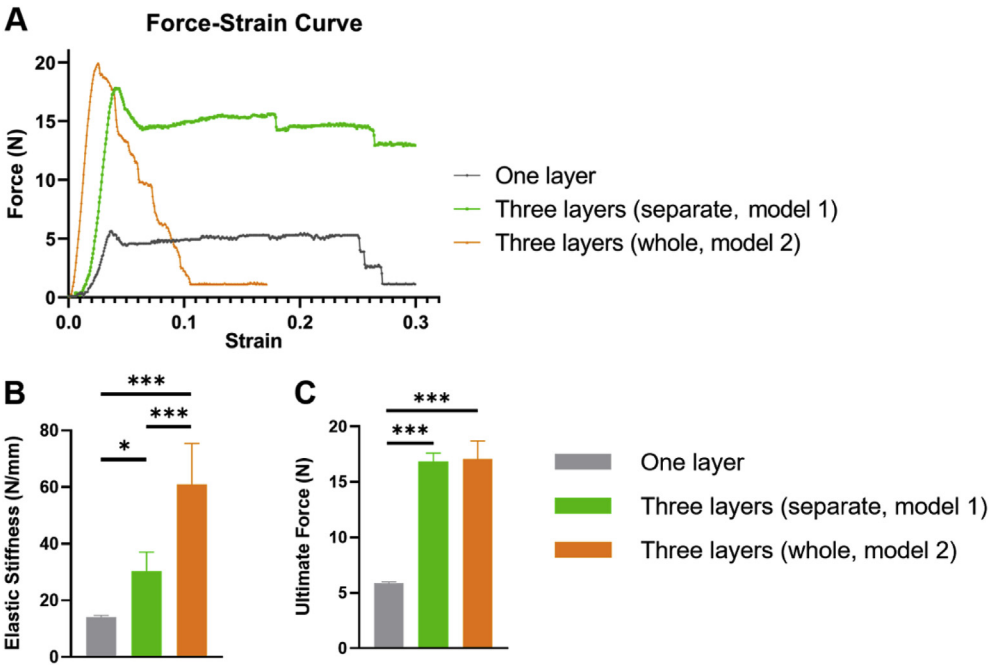

Fig. 3. Mechanical properties of the two types of multilayered scaffolds and one-layer PLGA scaffold. (A) Force-strain curve. (B) Elastic stiffness. (C) Ultimate force. One layer: one-layer PLGA scaffold; Three layers (separate, model 1): PLGA scaffolds with separate layer-by-layer structure; Three layers (whole, model 2): PLGA scaffolds with tri-layered structure. (n = 6, $*p < 0.05$, $***p < 0.001$).

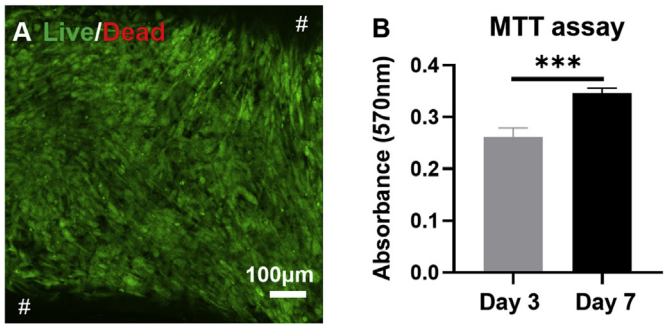

Fig. 4. The viability and proliferation tests of hADMSCs in the PLGA scaffold with collagen-fibrin hydrogel system. (A) Live/Dead image of hADMSCs at day 7. # in black background represented the middle frame of PLGA scaffolds. (B) The MTT assay of hADMSCs at day 3 and day 7 (n = 6; ***p < 0.001).

early marker expressed in large quantities with embryonic tendon [54]), TNMD, and collagen I (COL1) and collagen III (COLIII) (the most abundant collagen subtypes expressed in the tendon tissue [55]). The expressions of both SCX and TNMD were significantly increased after induction (Fig. 5B). COL3 was also upregulated in hADMSCs after culturing in TDM for 14 days, compared with those cultured in GM. These results demonstrated that the PLGA scaffold with the collagen-fibrin hydrogel supported the tenogenic differentiation of hADMSCs. During the culture and induction processes, the PLGA scaffold partially degraded, and the collagen-fibrin hydrogel became much thinner after culturing in the medium for 14 days. This is probably because we used PLGA (LA/GA = 50/50), which exhibits a fast degradation rate [56]. Previous studies also showed that, *in vitro*, the PLGA degradation rate accelerated after culturing for 6 days and resulted in substantial weight loss at day 14 [57,58]. The addition of other composites or materials might be a possible solution. It has been proven *in vitro* that the incorporation of wollastonite and bioglass 45S5 could both strongly affect the degradation rate of PLGA and reduce the side effects of the acidic degradation products of PLGA [59]. Future studies should be conducted to improve the stability of the scaffold and the durability of the hydrogel.

3.6. *In vivo* compatibility and degradability of two types of PLGA scaffolds with collagen-fibrin hydrogels

Two types of 3D printed multilayered PLGA scaffolds with collagen-fibrin hydrogels and without hADMSCs were subcutaneously implanted into the mice. Two weeks after surgery, the harvested scaffolds showed excellent tissue compatibility, with no severe inflammation for either model. The solid ends of the two types of scaffolds, i.e. separate layer-by-layer model and the tri-layered model, were surrounded by connective tissues (Fig. 6A and B). The solid ends were partially degraded, and for the middle part, more than 60% of the scaffolds were degraded and impaired when the scaffolds were harvested. Similarly to *in vitro* degradation, the *in vivo* degradation of the 3D printed scaffolds can also be further improved. For example, the hybridization of nano-apatitic particles demonstrated that it could effectively control the *in vivo* degradation rate and adverse effects of PLGA [60]. Another option is to blend the PLGA with other polymers that have slower degradation rates, like polycaprolactone (PCL), which remains intact for at least 2 years after implantation [61]. A combination of PLGA and PCL can effectively mitigate the rapid degradation rate of PLGA [62]. More durable materials need to be investigated for future studies in order to avoid scaffold deterioration before tendon or enthesis regeneration in the host body.

Currently, 3D printing has been widely implemented for tendon regeneration by using various biomaterials, developing novel structure designs, and combining stem cells or bioactive molecules. For example, decellularized extracellular matrix (dECM) and isolated collagen from dECM have been investigated as inks for 3D printing to regenerate tendon tissue because of their high degree of biomimicry [63,64]. The integration of poly-lactic acid (PLA) and collagen for 3D printing generated a scaffold with spatially tunable mechanical properties [65]. The application of bone morphogenic protein-12 (BMP-12)-overexpressing MSCs and a PLGA scaffold has been developed for rotator cuff repair, which resulted in enhanced tenogenic gene expression [66]. Novel strategies based on 3D printing have also been created to repair tendon defects, like electrohydrodynamic jet printing [67] and 3D-printed bone-anchoring bolts [68]. To further improve the outcome of rotator cuff tendon defects, biomimetic regeneration of the tendon-to-bone interface (i.e., enthesis) has become the new trend. In general, the tendon-to-bone interface has four different zones (i.e., tendon, non-

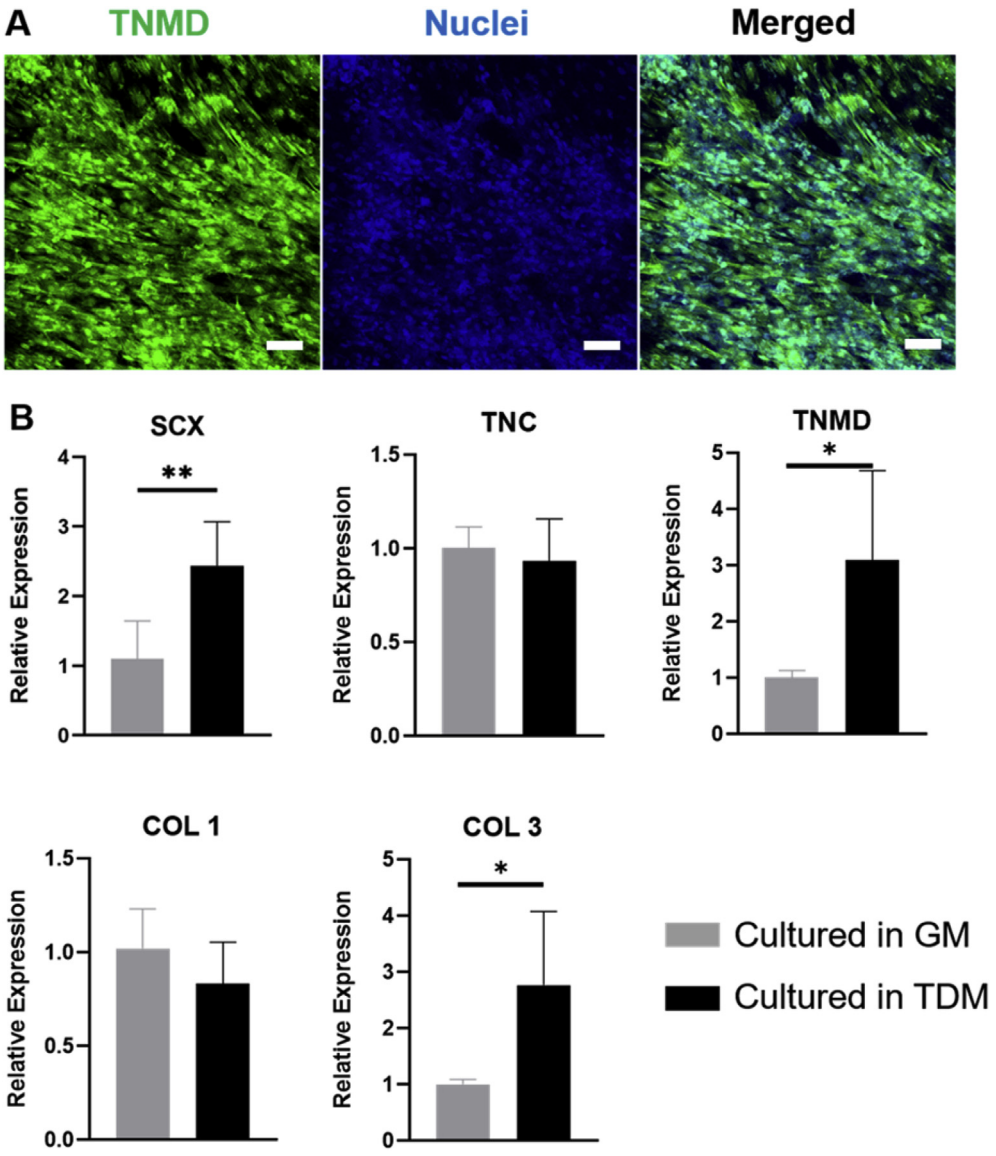

Fig. 5. Tenogenic differentiation of hADMSCs in the PLGA scaffold with collagen-fibrin hydrogel. (A) Immunofluorescent staining for TNMD (green) and nuclei (blue) of hADMSCs in the scaffold with hydrogel after 14-day culture in TDM. Scale bar = 100 μm. (B) Tendon-related genes expressions as normalized to 18s for both the control group culturing in GM for 14 days and the experimental group culturing in TDM for 14 days (n = 5, $*p < 0.05$, $**p < 0.01$).

mineralized fibrocartilage, mineralized fibrocartilage, and bone) [69]. Our current study demonstrates the feasibility of the fabrication of 3D printed multilayered scaffolds. Our future work will focus more on the material optimization to provide a balanced degradation rate and mechanical properties for application in enthesis regeneration. By using bioactive inorganic materials, like hydroxyapatite and β-tricalcium phosphate, we can also generate mineralized solid ends to promote the integration with bone ends. A 3D printed scaffold with spatiotemporal

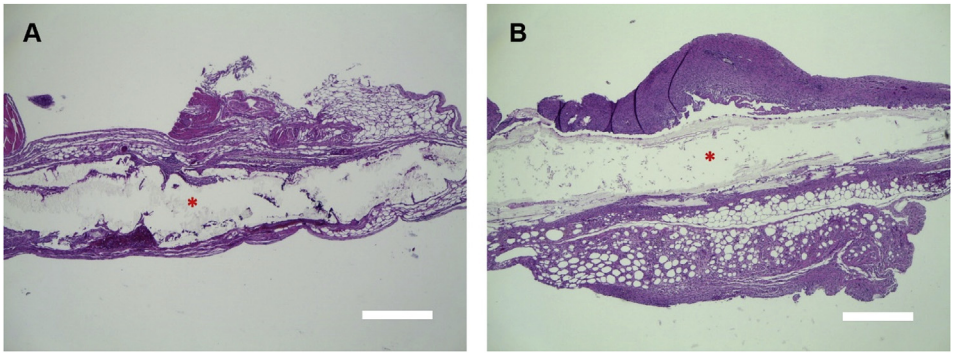

Fig. 6. H&E staining of two types of multilayered PLGA scaffolds with collagen-fibrin hydrogels after 2-week subcutaneous implantation. (A) Separate layer-by-layer model. (B) Tri-layered model. * represents the solid end of the scaffold model. Scale bar = 500 μm.

delivery of growth factors has been generated for fibrocartilaginous tendon-to-bone interface regeneration [70]. A biphasic hydrogel with mineralized and anisotropic features and encapsulated hADMSCs was developed for tendon and bone tissue reconstruction at the enthesis [71]. Therefore, our current work can be easily expanded with 3D printing/bioprinting of stem cells. For example, in our first model, three different regions (i.e. tendon, enthesis, and bone) can be 3D bioprinted by using hydrogels and hADMSCs, and then the printed layer can be sandwiched with a 3D printed polymer layer (like PLGA in this study or PLGA/PCL). The constructs will better mimic the tendon-to-bone structure and be expected to promote rotator cuff enthesis regeneration.

4. Conclusions

In this study, we designed and 3D printed two types of multilayered PLGA scaffolds with the incorporation of collagen-fibrin hydrogels and stem cells. The multilayered scaffolds with single-layered scaffold and hydrogel layers (first design) enable the further modification of different materials and cells and are easier to print, while the tri-layered scaffolds (second design) have better integration and are easier to use. Both types of multilayered scaffolds showed improved mechanical properties compared to the single-layered PLGA scaffold. The 3D printed PLGA scaffolds with collagen-fibrin hydrogels supported hADMSCs viability, proliferation, and tenogenic differentiation. The *in vivo* subcutaneous implantation showed that the multilayered scaffolds had excellent biocompatibility and *in vivo* degradability. Thus, both multilayered scaffolds have the potential for rotator cuff tendon-to-bone interface repair after further modification of material formulations.

CRediT authorship contribution statement

Xiping Jiang: Conceptualization, Methodology, Investigation, Writing - original draft. **Shaohua Wu:** Methodology, Investigation. **Mitchell Kuss:** Investigation, Writing - review & editing. **Yunfan Kong:** Investigation. **Wen Shi:** Investigation. **Philipp N. Streubel:** Conceptualization, Supervision. **Tieshi Li:** Conceptualization. **Bin Duan:** Conceptualization, Supervision, Writing - review & editing.

Declaration of competing interest

The authors declare that they have no known competing financial interests or personal relationships that could have appeared to influence the work reported in this paper.

Acknowledgements

This work has been supported by Mary & Dick Holland Regenerative Medicine Program start-up grant and pilot grant, Nebraska Research Initiative Funding, NIH (R01 AR073225) to B.D. and P.S. X.J is partially supported by the China Scholarship Council. The author wants to thank the Electron Microscopy Core Facility (EMCF) and Tissue Science Facility (TSF) at UNMC for technical assistance.

References

[1] J.S. Sher, J.W. Uribe, A. Posada, B.J. Murphy, M.B. Zlatkin, Abnormal findings on magnetic resonance images of asymptomatic shoulders, J Bone Joint Surg Am 77 (1) (1995) 10–15.
[2] K. Yamaguchi, K. Ditsios, W.D. Middleton, C.F. Hildebolt, L.M. Galatz, S.A. Teefey, The demographic and morphological features of rotator cuff disease. A comparison of asymptomatic and symptomatic shoulders, J Bone Joint Surg Am 88 (8) (2006) 1699–1704.
[3] L.S. Oh, B.R. Wolf, M.P. Hall, B.A. Levy, R.G. Marx, Indications for rotator cuff repair: a systematic review, Clin. Orthop. Relat. Res. 455 (2007) 52–63.
[4] D.A. van der Windt, B.W. Koes, B.A. de Jong, L.M. Bouter, Shoulder disorders in general practice: incidence, patient characteristics, and management, Ann. Rheum. Dis. 54 (12) (1995) 959–964.
[5] E. Maman, C. Harris, L. White, G. Tomlinson, M. Shashank, E. Boynton, Outcome of nonoperative treatment of symptomatic rotator cuff tears monitored by magnetic resonance imaging, J Bone Joint Surg Am 91 (8) (2009) 1898–1906.
[6] H.M. Kim, N. Dahiya, S.A. Teefey, W.D. Middleton, G. Stobbs, K. Steger-May, K. Yamaguchi, J.D. Keener, Location and initiation of degenerative rotator cuff tears: an analysis of three hundred and sixty shoulders, J Bone Joint Surg Am 92 (5) (2010) 1088–1096.
[7] C.D. Jarrett, C.C. Schmidt, Arthroscopic treatment of rotator cuff disease, J Hand Surg Am 36 (9) (2011) 1541–1552.
[8] C.C. Schmidt, C.D. Jarrett, B.T. Brown, Management of rotator cuff tears, J Hand Surg Am 40 (2) (2015) 399–408.
[9] B.R. Neri, K.W. Chan, Y.W. Kwon, Management of massive and irreparable rotator cuff tears, J. Shoulder Elbow Surg. 18 (5) (2009) 808–818.
[10] G. Diebold, P. Lam, J. Walton, G.A.C. Murrell, Relationship between age and rotator cuff retear: a study of 1,600 consecutive rotator cuff repairs, J Bone Joint Surg Am 99 (14) (2017) 1198–1205.
[11] Y.S. Lee, J.Y. Jeong, C.-D. Park, S.G. Kang, J.C. Yoo, Evaluation of the risk factors for a rotator cuff retear after repair surgery, Am. J. Sports Med. 45 (8) (2017) 1755–1761.
[12] J.H. Oh, M.S. Park, S.M. Rhee, Treatment strategy for irreparable rotator cuff tears, Clin. Orthop. Surg. 10 (2) (2018) 119–134.
[13] N.S. Cho, J.W. Yi, Y.G. Rhee, Arthroscopic biceps augmentation for avoiding undue tension in repair of massive rotator cuff tears, Arthroscopy 25 (2) (2009) 183–191.
[14] S.W. Mun, J.Y. Kim, S.H. Yi, C.H. Baek, Latissimus dorsi transfer for irreparable subscapularis tendon tears, J. Shoulder Elbow Surg. 27 (6) (2018) 1057–1064.
[15] R.J. Gillespie, D.M. Knapik, O. Akkus, Biologic and synthetic grafts in the reconstruction of large to massive rotator cuff tears, J. Am. Acad. Orthop. Surg. 24 (12) (2016) 823–828.
[16] T.W. Gilbert, J.M. Freund, S.F. Badylak, Quantification of DNA in biologic scaffold materials, J. Surg. Res. 152 (1) (2009) 135–139.
[17] V. Cirillo, J. Bushman, V. Guarino, J. Kohn, L. Ambrosio, 3D Conduits for Peripheral Nerve Regeneration, Electrofluidodynamic Technologies (EFDTs) for Biomaterials and Medical Devices, (2018), pp. 329–349 Elsevier.
[18] S.G. Sclamberg, J.E. Tibone, J.M. Itamura, S. Kasraeian, Six-month magnetic resonance imaging follow-up of large and massive rotator cuff repairs reinforced with porcine small intestinal submucosa, J. Shoulder Elbow Surg. 13 (5) (2004) 538–541.
[19] S. Zhao, W. Su, V. Shah, D. Hobson, L. Yildirimer, K.W.K. Yeung, J. Zhao, W. Cui, X. Zhao, Biomaterials based strategies for rotator cuff repair, Colloids Surf. B Biointerfaces 157 (2017) 407–416.
[20] N. Saveh-Shemshaki, L.S. Nair, C.T. Laurencin, Nanofiber-based matrices for rotator cuff regenerative engineering, Acta Biomater. 94 (2019) 64–81.
[21] F. Veronesi, V. Borsari, D. Contartese, J. Xian, N. Baldini, M. Fini, The clinical strategies for tendon repair with biomaterials: a review on rotator cuff and Achilles tendons, J. Biomed. Mater. Res. B Appl. Biomater. (2019), https://doi.org/10.1002/jbm.b.34525.
[22] T. Funakoshi, T. Majima, N. Iwasaki, N. Suenaga, N. Sawaguchi, K. Shimode, A. Minami, K. Harada, S.-i. Nishimura, Application of tissue engineering techniques for rotator cuff regeneration using a chitosan-based hyaluronan hybrid fiber scaffold, Am. J. Sports Med. 33 (8) (2005) 1193–1201.
[23] C.K. Hee, J.S. Dines, D.M. Dines, C.M. Roden, L.A. Wisner-Lynch, A.S. Turner, K.C. McGilvray, A.S. Lyons, C.M. Puttlitz, B.G. Santoni, Augmentation of a rotator cuff suture repair using rhPDGF-BB and a type I bovine collagen matrix in an ovine model, Am. J. Sports Med. 39 (8) (2011) 1630–1639.
[24] P.A. Janmey, J.P. Winer, J.W. Weisel, Fibrin gels and their clinical and bioengineering applications, J. R. Soc. Interface 6 (30) (2009) 1–10.
[25] B. Kundu, R. Rajkhowa, S.C. Kundu, X. Wang, Silk fibroin biomaterials for tissue regenerations, Adv. Drug Deliv. Rev. 65 (4) (2013) 457–470.
[26] A. Inui, T. Kokubu, H. Fujioka, I. Nagura, R. Sakata, H. Nishimoto, M. Kotera, T. Nishino, M. Kurosaka, Application of layered poly (L-lactic acid) cell free scaffold in a rabbit rotator cuff defect model, Sports Med. Arthrosc. Rehabil. Ther. Technol. 3 (2011) 29.
[27] K.L. Moffat, A.S.P. Kwei, J.P. Spalazzi, S.B. Doty, W.N. Levine, H.H. Lu, Novel nanofiber-based scaffold for rotator cuff repair and augmentation, Tissue Eng. 15 (1) (2009) 115–126.
[28] J. Xie, X. Li, J. Lipner, C.N. Manning, A.G. Schwartz, S. Thomopoulos, Y. Xia, Aligned-to-random" nanofiber scaffolds for mimicking the structure of the tendon-to-bone insertion site, Nanoscale 2 (6) (2010) 923–926.
[29] B.G. Santoni, K.C. McGilvray, A.S. Lyons, M. Bansal, A.S. Turner, J.D. Macgillivray, S.H. Coleman, C.M. Puttlitz, Biomechanical analysis of an ovine rotator cuff repair via porous patch augmentation in a chronic rupture model, Am. J. Sports Med. 38 (4) (2010) 679–686.
[30] C.M. O'Brien, B. Holmes, S. Faucett, L.G. Zhang, Three-dimensional printing of nanomaterial scaffolds for complex tissue regeneration, Tissue Eng. B Rev. 21 (1) (2015) 103–114.
[31] A.-V. Do, B. Khorsand, S.M. Geary, A.K. Salem, 3D printing of scaffolds for tissue regeneration applications, Adv Healthc Mater 4 (12) (2015) 1742–1762.
[32] T.K. Merceron, Y.-J. Burt M Fau - Seol, H.-W. Seol Yj Fau - Kang, S.J. Kang Hw Fau - Lee, J.J. Lee Sj Fau - Yoo, A. Yoo Jj Fau - Atala, A. Atala, A 3D Bioprinted Complex Structure for Engineering the Muscle-Tendon Unit, (1758-5090 (Electronic)).
[33] Y. Wang, S. Wu, M.A. Kuss, P.N. Streubel, B. Duan, Effects of hydroxyapatite and hypoxia on chondrogenesis and hypertrophy in 3D bioprinted ADMSC laden constructs, ACS Biomater. Sci. Eng. 3 (5) (2017) 826–835.
[34] M.R. Iaquinta, E. Mazzoni, M. Manfrini, A. D'Agostino, L. Trevisiol, R. Nocini, L. Trombelli, G. Barbanti-Brodano, F. Martini, M.A.-O. Tognon, Innovative Biomaterials for Bone Regrowth. LID - 10.3390/ijms20030618 [doi] LID - 618,

(1422-67 (Electronic)).
[35] S.T. Bianco, H.L. Moser, L.M. Galatz, A.H. Huang, Biologics and stem cell-based therapies for rotator cuff repair, Ann. N. Y. Acad. Sci. 1442 (1) (2019) 35–47.
[36] R. Costa-Almeida, I. Calejo, M.E. Gomes, Mesenchymal stem cells empowering tendon regenerative therapies, Int. J. Mol. Sci. 20 (12) (2019) 3002.
[37] A. Vinhas, M.T. Rodrigues, M.E. Gomes, Exploring stem cells and inflammation in tendon repair and regeneration, Adv. Exp. Med. Biol. 1089 (2018) 37–46.
[38] D.N. Heo, M. Hospodiuk, I.T. Ozbolat, Synergistic interplay between human MSCs and HUVECs in 3D spheroids laden in collagen/fibrin hydrogels for bone tissue engineering, Acta Biomater. 95 (2019) 348–356.
[39] S.L. Rowe, J.P. Stegemann, Interpenetrating collagen-fibrin composite matrices with varying protein contents and ratios, Biomacromolecules 7 (11) (2006) 2942–2948.
[40] L. Wei, S. Wu, M. Kuss, X. Jiang, R. Sun, P. Reid, X. Qin, B. Duan, 3D Printing of Silk Fibroin-Based Hybrid Scaffold Treated with Platelet Rich Plasma for Bone Tissue Engineering, (2452-199X (Electronic)).
[41] S. Wu, B. Duan, P. Liu, C. Zhang, X. Qin, J.T. Butcher, Fabrication of aligned nanofiber polymer yarn networks for anisotropic soft tissue scaffolds, ACS Appl. Mater. Interfaces 8 (26) (2016) 16950–16960.
[42] S. Wu, H. Peng, X. Li, P.N. Streubel, Y. Liu, B. Duan, Effect of scaffold morphology and cell co-culture on tenogenic differentiation of HADMSC on centrifugal melt electrospun poly (L-lactic acid) fibrous meshes, Biofabrication 9 (4) (2017) 044106.
[43] S. Wu, Y. Wang, P.N. Streubel, B. Duan, Living nanofiber yarn-based woven biotextiles for tendon tissue engineering using cell tri-culture and mechanical stimulation, Acta Biomater. 62 (2017) 102–115.
[44] M.A. Kuss, S. Wu, Y. Wang, J.B. Untrauer, W. Li, J.Y. Lim, B. Duan, Prevascularization of 3D printed bone scaffolds by bioactive hydrogels and cell co-culture, J. Biomed. Mater. Res. B Appl. Biomater. 106 (5) (2018) 1788–1798.
[45] V. Dumas, L. Guignandon A Fau - Vico, C. Vico L Fau - Mauclair, X. Mauclair C Fau - Zapata, M.T. Zapata X Fau - Linossier, W. Linossier Mt Fau - Bouleftour, J. Bouleftour W Fau - Granier, S. Granier J Fau - Peyroche, J.-C. Peyroche S Fau - Dumas, H. Dumas Jc Fau - Zahouani, A. Zahouani H Fau - Rattner, A. Rattner, Femtosecond Laser Nano/micro Patterning of Titanium Influences Mesenchymal Stem Cell Adhesion and Commitment, (1748-605X (Electronic)).
[46] H. Jeon, G. Simon Cg Jr Fau - Kim, G. Kim, A Mini-Review: Cell Response to Microscale, Nanoscale, and Hierarchical Patterning of Surface Structure, (1552-4981 (Electronic)).
[47] A.R. Sadeghi, S. Nokhasteh, A.M. Molavi, M. Khorsand-Ghayeni, H. Naderi-Meshkin, A. Mahdizadeh, Surface Modification of Electrospun PLGA Scaffold with Collagen for Bioengineered Skin Substitutes, (1873), p. 191 (Electronic)).
[48] W. Wang, Y. Li B Fau - Li, Y. Li Y Fau - Jiang, H. Jiang Y Fau - Ouyang, C. Ouyang H Fau - Gao, C. Gao, In Vivo Restoration of Full-Thickness Cartilage Defects by Poly (lactide-Co-Glycolide) Sponges Filled with Fibrin Gel, Bone Marrow Mesenchymal Stem Cells and DNA Complexes, (1878), p. 5905 (Electronic)).
[49] R.R. Rao, J. Peterson Aw Fau - Ceccarelli, A.J. Ceccarelli J Fau - Putnam, J.P. Putnam Aj Fau - Stegemann, J.P. Stegemann, Matrix Composition Regulates Three-Dimensional Network Formation by Endothelial Cells and Mesenchymal Stem Cells in Collagen/fibrin Materials, (1573-7209 (Electronic)).
[50] C.L. Cummings, R.M. Gawlitta D Fau - Nerem, J.P. Nerem Rm Fau - Stegemann, J.P. Stegemann, Properties of Engineered Vascular Constructs Made from Collagen, Fibrin, and Collagen-Fibrin Mixtures, (0142-9612 (Print)).
[51] F.A. Barber, M.A. Herbert, M.H. Boothby, Ultimate tensile failure loads of a human dermal allograft rotator cuff augmentation, Arthroscopy 24 (1) (2008) 20–24.
[52] S. Pauly, B. Kieser, A. Schill, C. Gerhardt, M. Scheibel, Biomechanical comparison of 4 double-row suture-bridging rotator cuff repair techniques using different medial-row configurations, Arthroscopy 26 (10) (2010) 1281–1288.
[53] C.L. Mendias, J.P. Gumucio, K.I. Bakhurin, E.B. Lynch, S.V. Brooks, Physiological loading of tendons induces scleraxis expression in epitenon fibroblasts, J. Orthop. Res. 30 (4) (2012) 606–612.
[54] T.A. Järvinen, L. Jozsa, P. Kannus, T.L. Järvinen, M. Kvist, T. Hurme, J. Isola, H. Kalimo, M. Järvinen, Mechanical loading regulates tenascin-C expression in the osteotendinous junction, J. Cell Sci. 112 Pt 18 (1999) 3157–3166.
[55] M.B. Klein, N. Yalamanchi, H. Pham, M.T. Longaker, J. Chang, Flexor tendon healing in vitro: effects of TGF-beta on tendon cell collagen production, J Hand Surg Am 27 (4) (2002) 615–620.
[56] P. Gentile, V. Chiono, I. Carmagnola, V.P. Hatton, An overview of poly(lactic-co-glycolic) acid (PLGA)-Based biomaterials for bone tissue engineering, Int. J. Mol. Sci. 15 (3) (2014).
[57] L. Xiaoqiang, S. Yan, C. Rui, H. Chuanglong, W. Hongsheng, M. Xiumei, Fabrication and properties of core-shell structure P(LLA-CL) nanofibers by coaxial electrospinning, J. Appl. Polym. Sci. 111 (3) (2009) 1564–1570.
[58] X. Zong, S. Ran, K.-S. Kim, D. Fang, B.S. Hsiao, B. Chu, Structure and morphology changes during in vitro degradation of electrospun poly(glycolide-co-lactide) nanofiber membrane, Biomacromolecules 4 (2) (2003) 416–423.
[59] H. Li, J. Chang, pH-compensation effect of bioactive inorganic fillers on the degradation of PLGA, Compos. Sci. Technol. 65 (14) (2005) 2226–2232.
[60] W. Ji, F. Yang, H. Seyednejad, Z. Chen, W.E. Hennink, J.M. Anderson, J.J.J.P. van den Beucken, J.A. Jansen, Biocompatibility and degradation characteristics of PLGA-based electrospun nanofibrous scaffolds with nanoapatite incorporation, Biomaterials 33 (28) (2012) 6604–6614.
[61] H. Sun, L. Mei, C. Song, X. Cui, P. Wang, The in vivo degradation, absorption and excretion of PCL-based implant, Biomaterials 27 (9) (2006) 1735–1740.
[62] J.-H. Shim, T.-S. Moon, M.-J. Yun, Y.-C. Jeon, C.-M. Jeong, D.-W. Cho, J.-B. Huh, Stimulation of healing within a rabbit calvarial defect by a PCL/PLGA scaffold blended with TCP using solid freeform fabrication technology, J. Mater. Sci. Mater. Med. 23 (12) (2012) 2993–3002.
[63] A.D. Nocera, R. Comín, N.A. Salvatierra, M.P. Cid, Development of 3D Printed Fibrillar Collagen Scaffold for Tissue Engineering, (1572-8781 (Electronic)).
[64] B. Toprakhisar, A.A.-O. Nadernezhad, E.A.-O. Bakirci, N.A.-O. Khani, G.A. Skvortsov, B.A.-O. Koc, Development of Bioink from Decellularized Tendon Extracellular Matrix for 3D Bioprinting, (1616-5195 (Electronic)).
[65] L.C. Mozdzen, A. Vucetic, B.A.C. Harley, Modifying the Strength and Strain Concentration Profile within Collagen Scaffolds Using Customizable Arrays of Poly-Lactic Acid Fibers, (1878), p. 180 (Electronic)).
[66] P. Chen, L. Cui, G. Chen, T. You, W. Li, J. Zuo, C. Wang, W. Zhang, C. Jiang, The Application of BMP-12-Overexpressing Mesenchymal Stem Cells Loaded 3D-Printed PLGA Scaffolds in Rabbit Rotator Cuff Repair, (1879-0003 (Electronic)).
[67] Y. Wu, Z. Wang, J. Ying Hsi Fuh, Y. San Wong, W. Wang, E. San Thian, Direct E-Jet Printing of Three-Dimensional Fibrous Scaffold for Tendon Tissue Engineering, (1552-4981 (Electronic)).
[68] Y.C. Chou, W.L. Yeh, C.L. Chao, Y.H. Hsu, Y.H. Yu, J.K. Chen, S.J. Liu, Enhancement of Tendon-Bone Healing via the Combination of Biodegradable Collagen-Loaded Nanofibrous Membranes and a Three-Dimensional Printed Bone-Anchoring Bolt, (1178-2013 (Electronic)).
[69] S. Font Tellado, E.R. Balmayor, M. Van Griensven, Strategies to Engineer Tendon/ligament-To-Bone Interface: Biomaterials, Cells and Growth Factors, (1872) -8294 (Electronic)).
[70] S. Tarafder, S. Brito Ja Fau - Minhas, L. Minhas S Fau - Effiong, S. Effiong L Fau - Thomopoulos, C.H. Thomopoulos S Fau - Lee, C.H. Lee, In Situ Tissue Engineering of the Tendon-To-Bone Interface by Endogenous Stem/progenitor Cells, (1758-5090 (Electronic)).
[71] M.A.-O. Echave, R.A.-O. Domingues, M.A.-O. Gómez-Florit, J.L. Pedraz, R.L. Reis, G. Orive, M.E. Gomes, Biphasic Hydrogels Integrating Mineralized and Anisotropic Features for Interfacial Tissue Engineering, (1944), p. 8252 (Electronic)).